JOURNAL OF SPACECRAFT AND ROCKETS
Vol. 42, No. 5, September–October 2005

Prediction of the Pitch-Damping Coefficients Using Sacks's Relations

Paul Weinacht* and James E. Danberg†
U.S. Army Research Laboratory, Aberdeen Proving Ground, Maryland 21005

Throughout its development, slender-body theory has been generalized to predict a large variety of aerodynamic coefficients for a wide class of flight bodies. For most applications, slender-body theory provides only a qualitative predictive capability. There is, however, a set of slender-body relationships that have been previously derived by Sacks that allow the individual pitch-damping coefficients and the pitch-damping coefficient sums to be related to each other. Until recently, it has been difficult to assess the accuracy of these relationships because of the lack of high-quality pitch-damping data or the lack of a higher-order theory. The current work applies a recently developed computational fluid dynamics capability for predicting all three pitch-damping coefficients. From this analysis, the accuracy of these relationships has been assessed and their engineering significance demonstrated. One important result is that the pitch-damping relations developed by Sacks allow the individual pitch-damping coefficients to be determined from the pitch-damping coefficient sum with a high degree of accuracy.

Nomenclature

a	=	speed of sound
C_m	=	pitching-moment coefficient, $\bar{M}/\frac{1}{2}\rho_\infty V^2 S_{\text{ref}} D$
C_{m_q}	=	pitch-damping-moment coefficient slope due to body transverse angular rate, $\partial C_m/\partial(qD/V)$
$C_{m_q}+C_{m_{\dot\alpha}}$	=	pitch-damping-moment coefficient sum
C_{m_α}	=	pitching-moment coefficient slope with respect to angle of attack, $\partial C_m/\partial\alpha$
$C_{m_{\dot\alpha}}$	=	pitch-damping-moment coefficient slope due to angular rate associated with angle of attack, $\partial C_m/\partial(\dot\alpha D/V)$
$C_{2_{m_\alpha}}$	=	pitching-second-moment coefficient angle-of-attack slope, $\partial C_{2_m}/\partial\alpha$
C_N	=	normal-force coefficient, $\bar{F}/\frac{1}{2}\rho_\infty V^2 S_{\text{ref}}$
C_{N_q}	=	pitch-damping-force slope due to body transverse angular rate $\partial C_N/\partial(q_D/V)$
$C_{N_q}+C_{N_{\dot\alpha}}$	=	pitch-damping-force coefficient sum
C_{N_α}	=	normal-force coefficient slope with respect to angle of attack $\partial C_N/\partial\alpha$
$C_{N_{\dot\alpha}}$	=	pitch-damping-force coefficient slope due to angular rate associated with angle of attack $\partial C_N/\partial(\dot\alpha D/V)$
C_n	=	side-moment coefficient
D	=	reference diameter
$\hat{\boldsymbol{E}}, \hat{\boldsymbol{F}}, \hat{\boldsymbol{G}}$	=	flux vectors in transformed coordinates
e	=	total energy per unit volume
$\bar{F}$	=	force
$\hat{\boldsymbol{H}}$	=	source term in Navier–Stokes equations due to rotating coordinate frame
$\hat{\boldsymbol{H}}_c$	=	source term in Navier–Stokes equations due to cylindrical coordinates
L	=	body length
$\bar{M}$	=	moment
p	=	pressure
q	=	transverse angular rate of body as used in flight mechanics equations
$\boldsymbol{q}^T$	=	transposed vector of dependent variables as used in Navier–Stokes equations
Re	=	Reynolds number, $a_\infty\rho_\infty D/\mu_\infty$
R_0	=	helix radius
r	=	radial coordinate
S_{ref}	=	reference area, $\pi D^2/4$
$\hat{\boldsymbol{S}}$	=	viscous flux vector
$\hat{\boldsymbol{S}}_c$	=	viscous terms due to cylindrical coordinate formulation
U, V, W	=	contravariant velocity components
u, v, w	=	velocity components in the x, ϕ, r directions
V	=	freestream velocity
X_e, Y_e, Z_e	=	Earth-fixed coordinates
x	=	axial location along body from nose
x_{cg}	=	axial location of center of gravity from nose
$\bar{x}$	=	integration variable associated with axial location along body from nose
α	=	angle of attack
$\dot\alpha$	=	angular rate associated with angle of attack
γ	=	cosine of total angle of attack
δ	=	sine of total angle of attack
Δ	=	deviation or error in Sacks's relations for force
$\bar\Delta$	=	deviation or error in Sacks's relations for moment
μ	=	viscosity
ξ, η, ζ	=	transformed coordinates in the Navier–Stokes equations
ρ	=	density
ϕ	=	circumferential coordinate
Ω	=	angular rate associated with coning and helical motions
ω	=	angular velocity about longitudinal axis

Subscript

∞	=	quantity evaluated at freestream conditions

Presented as Paper 2003-5467 at the AIAA Atmospheric Flight Mechanics Conference, Austin, TX, 11–14 August 2003; received 7 May 2004; revision received 24 November 2004; accepted for publication 29 November 2004.

*Aerospace Engineer, Aerodynamics Branch, Weapons and Materials Research Directorate. Associate Fellow AIAA.

†ARL Guest Researcher; also Professor Emeritus, Department of Mechanical Engineering, University of Delaware, Newark, DE 19716. Associate Fellow AIAA.

Introduction

THE pitch-damping-moment coefficients C_{m_q} (due to body transverse angular rate) and $C_{m_{\dot\alpha}}$ (due to angular rate associated with angle of attack) play an important role in the performance and dynamic stability of flight bodies. The pitch-damping-moment coefficient sum $C_{m_q}+C_{m_{\dot\alpha}}$ is of most practical importance, although the individual damping coefficients are often required in aerodynamic analyses. Throughout the past several decades, a variety of

techniques and theories have been developed for predicting the pitch-damping coefficients.[1–10] These techniques vary in their ease of use as well as their ability to accurately predict the pitch-damping coefficients.

During the course of its development, slender-body theory was generalized to predict a large variety of aerodynamic coefficients including the pitch-damping coefficients.[1,2] In general, direct application of these methods provides only qualitative results for the aerodynamic coefficients. However, elements of slender-body theory have been incorporated into current engineering methods. These methods[3–5] have evolved considerably, although their implementation is fairly complex. Apart from implementation issues, modern engineering methods, once embodied into a computer code, are relatively easy to use and provide fast and reasonably accurate aerodynamic predictions for a large variety of flight geometries.

From slender-body theory, some important relationships between the various aerodynamic coefficients can be derived, although these relationships only hold rigorously within the context of theories from which they were obtained. Bryson[2] derived the relatively well-known slender-body result that relates the pitch-damping-moment coefficient sum to the normal-force coefficient, shown in Eq. (1):

$$C_{m_q} + C_{m_{\dot\alpha}} = -[(L - x_{\mathrm{cg}})/D]^2 C_{N_\alpha} \tag{1}$$

Sacks,[1] using the Blasius method for calculating the forces and moments on slender bodies from the crossflow potential, found that many of the aerodynamic coefficients were related to each other. Sacks obtained expressions that directly related the individual pitch-damping coefficients to the normal-force coefficient, such as the pitch-damping-force coefficient shown in Eq. (2). These expressions have a form similar to Bryson's result shown in Eq. (1):

$$C_{N_q} = [(L - x_{\mathrm{cg}})/D] C_{N_\alpha} \tag{2}$$

In practice, these relations that directly relate the damping coefficients to the normal-force coefficient do not perform particularly well, even when the slender-body evaluation of the normal-force coefficient is replaced with a more accurate evaluation of the normal-force coefficient from sources such as experimental measurement or computational fluid dynamics (CFD).[6] However, these relations can be combined with empirical corrections to yield more reliable results.[6,7]

Sacks also found expressions that related the individual damping coefficients to each other, including the following relationship between the pitch-damping-force coefficients:

$$C_{N_q} = C_{N_{\dot\alpha}} - C_{m_\alpha} \tag{3}$$

Sacks's explicitly derived relation shown in Eq. (3) can be easily generalized using his theory to the individual pitch-damping-force and -moment coefficients and the pitch-damping-force and -moment sums as shown in Eqs. (4–9). For the purposes of this paper, these relationships will be referred to as Sacks's relations:

$$C_{N_q} = C_{N_{\dot\alpha}} - C_{m_\alpha} \tag{4}$$

$$C_{m_q} = C_{m_{\dot\alpha}} - C_{2m_\alpha} \tag{5}$$

$$\left[C_{N_q} + C_{N_{\dot\alpha}}\right] = 2C_{N_{\dot\alpha}} - C_{m_\alpha} \tag{6}$$

$$\left[C_{m_q} + C_{m_{\dot\alpha}}\right] = 2C_{m_{\dot\alpha}} - C_{2m_\alpha} \tag{7}$$

$$\left[C_{N_q} + C_{N_{\dot\alpha}}\right] = 2C_{N_q} + C_{m_\alpha} \tag{8}$$

$$\left[C_{m_q} + C_{m_{\dot\alpha}}\right] = 2C_{m_q} + C_{2m_\alpha} \tag{9}$$

Sacks's contribution is the recognition that these relationships exist, although the same relations are implicitly contained in other theories such as that presented by Bryson.[2]

For slender bodies, these relations are independent of configuration and are applicable to both winged and wingless bodies. The importance of these relationships is that if just one of the three pitch-damping-force (or moment) coefficients can be determined (C_{N_q}, $C_{N_{\dot\alpha}}$ or $[C_{N_q} + C_{N_{\dot\alpha}}]$), the other two damping coefficients can be obtained using simple closed-form expressions. This, of course, assumes that the pitching-moment coefficient C_{m_α} (first moment of the normal force) and the second moment of normal force C_{2m_α} can be obtained as well. Both of these coefficients can be obtained if the normal-force distribution is known as shown in Eqs. (10) and (11):

$$C_{m_\alpha} = \int_0^x \frac{(x_{\mathrm{cg}} - \bar{x})}{D} \frac{\mathrm{d}C_{N_\alpha}}{\mathrm{d}\bar{x}}\,\mathrm{d}\bar{x} \tag{10}$$

$$C_{2m_\alpha} = \int_0^x \frac{(x_{\mathrm{cg}} - \bar{x})^2}{D^2} \frac{\mathrm{d}C_{N_\alpha}}{\mathrm{d}\bar{x}}\,\mathrm{d}\bar{x} \tag{11}$$

Predictive methods for the static normal force and static pitching moment are well established, even for fast-design methods.

Because Sacks's relations were derived using simple approximate theories, it remains to be shown whether the validity of the relations shown in Eqs. (4–9) exists only within the context of the theories from which they were derived or whether they are universally valid for slender bodies, or perhaps, more importantly, whether they are of general engineering significance. The preceding relations in Eqs. (4–9) differ somewhat from the results in Eqs. (1) and (2) because they relate the pitch-damping coefficients to each other rather than purely to the static normal-force coefficient. This suggests that Sacks's relations might more properly represent the physics compared to their counterparts that directly relate the damping coefficients to the normal-force coefficient. Because of this, there is reason to investigate the validity and accuracy of Sacks's relations.

Recently, a computational approach for predicting all three of the pitch-damping coefficients has been developed.[8,9] The approach solves the three-dimensional thin-layer Navier–Stokes equations for three different imposed motions that allow the three pitch-damping coefficients to be predicted independently. The pitch-damping-force and -moment coefficient sums are determined from the computation of a body undergoing an imposed coning motion.[8] The individual pitch-damping coefficients are obtained from computations of a body undergoing two specific types of imposed helical motions.[9] Each of these motions is described in the following sections. One of the key components of this method is that steady flow techniques can be employed to predict aerodynamic derivatives normally associated with time-dependent motions.

Using the computational approach, the validity, accuracy, and applicability of Sacks's relations are assessed in the current paper. A brief description of the helical and coning motions used to generate the pitch-damping coefficients of interest are presented in the following two sections, followed by a section discussing the computational approach. Results are then presented examining the performance of Sacks's relations for two axisymmetric body geometries.

Helical Motions and the Individual Pitch-Damping Coefficients

Forces and moments related to the two individual rates q and $\dot\alpha$ can be excited independently using two types of motion in which the center of gravity of the flight vehicle traverses a helical flight path. The first motion requires the vehicle's longitudinal axis to be oriented in the same direction as the center of rotation of the helix but displaced by a constant distance. Figure 1 shows a three-dimensional view of the motion.

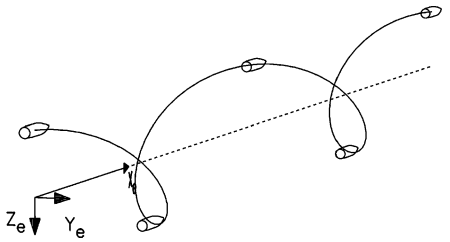

Fig. 1 Helical motion with nonzero $\dot\alpha$ and zero q.

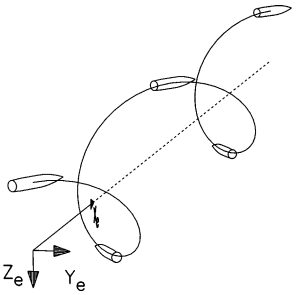

Fig. 2 Helical motion with zero $\dot{\alpha}$ and nonzero q.

This particular motion produces no rotation of the body-fixed nonrolling coordinate frame relative to an Earth-fixed coordinate frame, and hence the transverse angular velocity of the body is zero. The angle of attack and its angular rate vary continuously, producing moment components associated with the coefficients C_{m_α} and $C_{m_{\dot{\alpha}}}$, respectively. This motion is referred to as $q = 0$ helical motion because the angular rates associated with the damping coefficient C_{m_q} are zero.

For the second motion, the longitudinal axis of the flight vehicle remains tangent to the helical flight path at each point along the trajectory. Figure 2 shows a three-dimensional view of this motion. The angle of attack of the incident airstream is zero because both the longitudinal axis of the body and the freestream velocity vector are tangent to the flight path. The resulting yawing rate is also zero because the angle of attack is constant. The angular orientation of the flight body changes continuously with respect to an Earth-fixed reference frame, producing a nonzero transverse angular rate. As a result, moment components associated with the damping-moment coefficient C_{m_q} are produced. This motion is referred to as $\dot{\alpha} = 0$ helical motion because the angular rates associated with the damping coefficient $C_{m_{\dot{\alpha}}}$ are zero.

For each of the helical motions, the transverse aerodynamic moment in the nonrolling frame will be periodic in time, which also indicates that the flowfield will be periodic in time when viewed from the nonrolling coordinate frame. The time dependency is removed by transforming to an orthogonal right-handed coordinate system that has its x axis aligned with the longitudinal axis of the body and its z axis along a line between the body c.g. and the axis of rotation of the helix.

For each of the helical motions already described, the spin rate of the body has not been defined. To eliminate any contributions to the aerodynamic forces and moments from the Magnus forces and moments, the spin rate is fixed to zero (see Refs. 8 and 9 for details). The resulting in-plane moment C_m and side moment C_n coefficients in the transformed coordinate system for both types of helical motions are shown in Eqs. (12) and (13).

Zero-spin $q = 0$ helical motion:

$$C_m + iC_n = -C_{m_{\dot{\alpha}}}(\Omega D/V)(R_0\Omega/V) + iC_{m_\alpha}(R_0\Omega/V) \qquad (12)$$

Zero-spin $\dot{\alpha} = 0$ helical motion:

$$C_m + iC_n = C_{m_q}(\Omega D/V)(R_0\Omega/V) \qquad (13)$$

Here, Ω is the angular velocity of the body about the helix axis, R_0 is the perpendicular distance between the helix axis and the body c.g., and V is the total linear velocity of the c.g. Similar expressions for the individual damping-force coefficients can be developed using the same approach as applied for the moment coefficients. A more complete discussion of the helical motions, the transformed coordinate system, and the transverse force and moment equations is contained in Ref. 9.

Coning Motion and the Pitch-Damping Sum

To predict the pitch-damping coefficient sum, coning motion is employed. In steady coning motion, the longitudinal axis of the flight body performs a rotation at a constant angular velocity about a line parallel to the freestream velocity vector and coincident with the body's c.g., while oriented at a constant angle with respect to the freestream velocity vector. This is shown schematically in Fig. 3. In the context of this paper, coning motion also requires the c.g. to traverse a rectilinear path at constant velocity such that the freestream velocity vector has a fixed orientation with the inertial frame.

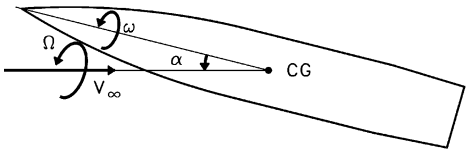

Fig. 3 Schematic of coning motion.

Relative to a nonrolling coordinate frame, both the transverse angular rate of the body and the angular rate associated with angle of attack vary in a periodic manner, thereby exciting the aerodynamic forces and moments associated with both of the individual pitch-damping coefficients. Here, a specific form of coning motion, described as zero-spin coning motion, is employed. In zero-spin coning motion, the total angular velocity of the body along the longitudinal axis (the spin rate) is zero. By imposing zero spin rate on the body, the contributions from the Magnus forces and moments are eliminated.

The time dependency is removed by transforming the body-fixed nonrolling coordinate frame to an orthogonal right-handed coordinate system that has its x axis aligned with the longitudinal axis of the body and its z axis in the pitch plane of the body. Within this transformed coordinate frame, in-plane moment C_m and side-moment C_n coefficients have the following form.

Zero-spin coning motion:

$$C_m + iC_n = i\delta(\Omega D/V)\left[C_{m_q} + \gamma C_{m_{\dot{\alpha}}}\right] + C_{m_\alpha}\delta \qquad (14)$$

Here, the side moment is proportional to the pitch-damping-moment coefficient sum and varies linearly with the coning rate Ω and sine of the total angle of attack δ. For small angles of attack, the cosine of the total angle of attack γ can be assumed to be one. A more complete discussion of the coning motion, the transformed coordinate system and the transverse force and moment equations is contained in Ref. 8.

The pitch-damping coefficient sum can also be determined by simply adding the individual damping coefficients. In practice, there is very little difference in the two results.[9] However, for the current study, directly predicting the pitch-damping coefficient sum using coning motion provides an alternative prediction of the pitch-damping sum and additional confirmation of the predictions of the individual coefficients.

Computational Technique

In the preceding sections, several types of steady motion that produce aerodynamic forces and moments from which the various pitch-damping coefficients can be obtained were presented. One unique feature of these motions is that they are steady motions. The advantage of a steady motion over an unsteady motion is that a potentially time-independent flowfield can be produced by a steady motion, permitting analysis using steady flow CFD techniques. Such techniques can be computationally less expensive than time-dependent CFD approaches. To fully exploit the steady character of the flow, special body-fixed coordinate systems have been employed to capture the steady flowfield. One feature of these coordinate frames is that they are rotating at a constant rate with respect to an inertial frame. Because of this, the governing equations of fluid motion must be modified to take into account the centrifugal and Coriolis force terms associated with the noninertial rotating frame.

The steady thin-layer Navier–Stokes equations are shown in Eq. (15):

$$\frac{\partial \hat{\boldsymbol{E}}}{\partial \xi} + \frac{\partial \hat{\boldsymbol{F}}}{\partial \eta} + \frac{\partial \hat{\boldsymbol{G}}}{\partial \zeta} + \hat{\boldsymbol{H}}_c + \hat{\boldsymbol{H}} = \frac{1}{Re}\left(\frac{\partial \hat{\boldsymbol{S}}}{\partial \zeta} + \hat{\boldsymbol{S}}_c\right) \qquad (15)$$

The inviscid flux vectors $\hat{\boldsymbol{E}}$, $\hat{\boldsymbol{F}}$, and $\hat{\boldsymbol{G}}$; the viscous term $\hat{\boldsymbol{S}}$; the inviscid and viscous source terms due to the cylindrical coordinate

formulation $\hat{\boldsymbol{H}}_c$ and $\hat{\boldsymbol{S}}_c$; and the source term containing the Coriolis and centrifugal force terms that result from the rotating coordinate frame $\hat{\boldsymbol{H}}$ are functions of the dependent variables represented by the vector $\boldsymbol{q}^T = (\rho, \rho u, \rho v, \rho w, e)$, where u, v, and w are the velocity components in axial, circumferential, and normal directions. The inviscid flux vectors and the source term due to the rotating coordinate frame are shown in Eq. (16). Details of the thin-layer viscous term and the source terms due to the cylindrical coordinate formulation are available in Refs. 11 and 12, respectively:

$$\hat{\boldsymbol{E}} = \frac{1}{J}\begin{bmatrix} \rho U \\ \rho u U + \xi_x p \\ \rho v U \\ \rho w U \\ (e+p)U \end{bmatrix} \qquad \hat{\boldsymbol{F}} = \frac{1}{J}\begin{bmatrix} \rho V \\ \rho u V + \eta_x p \\ \rho v V + \eta_\phi p/r \\ \rho w V + \eta_r p \\ (e+p)V \end{bmatrix}$$

$$\hat{\boldsymbol{G}} = \frac{1}{J}\begin{bmatrix} \rho W \\ \rho u W + \zeta_x p \\ \rho v W + \zeta_\phi p/r \\ \rho w W + \zeta_r p \\ (e+p)W \end{bmatrix} \qquad \hat{\boldsymbol{H}} = \frac{1}{J}\begin{bmatrix} 0 \\ \rho f_x \\ \rho f_\phi \\ \rho f_r \\ \rho u f_x + \rho v f_\phi + \rho w f_r \end{bmatrix} \tag{16}$$

The pressure p can be related to the dependent variables by applying the ideal-gas law:

$$p = (\gamma - 1)[e - (\rho/2)(u^2 + v^2 + w^2)] \tag{17}$$

The turbulent viscosity μ_t, which appears in the viscous matrices, was computed using the Baldwin–Lomax turbulence model.[13]

The Coriolis and centrifugal acceleration terms due to the rotating coordinate system, which are contained in the source term $\hat{\boldsymbol{H}}$, are shown in Eq. (18):

$$\boldsymbol{f} = 2\boldsymbol{\Omega} \times \boldsymbol{u} + \boldsymbol{\Omega} \times (\boldsymbol{\Omega} \times \boldsymbol{R}) \tag{18}$$

The Coriolis acceleration is a function of the angular velocity of the coordinate frame with respect to the inertial frame $\boldsymbol{\Omega}$ and the fluid velocity vector $\boldsymbol{u}$, which can be represented by the velocity components u, v, and w. The centripedal acceleration is a function of the angular velocity of the rotating frame $\boldsymbol{\Omega}$ and the displacement vector $\boldsymbol{R}$ between the axis of rotation and the local position in the flowfield. The acceleration vector $\boldsymbol{f}$ can be written in terms of its components along the x, ϕ, and r axes, f_x, f_ϕ and f_r.

The steady thin-layer equations are solved using the parabolized Navier–Stokes technique of Schiff and Steger.[11] This "space-marching" approach integrates the governing equations from the nose of the flight body to the tail. Following the approach of Schiff and Steger, the governing equations, which have been modified here to include the Coriolis and centrifugal force terms, are solved using a conservative, approximately factored, implicit finite difference numerical algorithm as formulated by Beam and Warming.[14] Details of the implementation of the source term that contains the Coriolis and centrifugal force terms are given in Refs. 8 and 9.

The technique has been validated with available experimental data where possible, and excellent agreement is found.[8,15] Grid-resolution studies were also performed in the original studies to ensure grid-independent solutions.[8,9]

Results

In the current context, this computational procedure allows the general applicability of Sacks's pitch-damping relations to be examined. Arguably, up to now, it has not been possible to assess the validity or accuracy of these relationships because of the uncertainty associated with experimentally derived pitch-damping data and the lack of a higher-order theory. In the current research effort, the technique has been applied to two axisymmetric body geometries: an ogive-cylinder configuration and a cone-cylinder body with a flared afterbody. The accuracy of Sacks's relations is examined for each of these body geometries in supersonic flight.

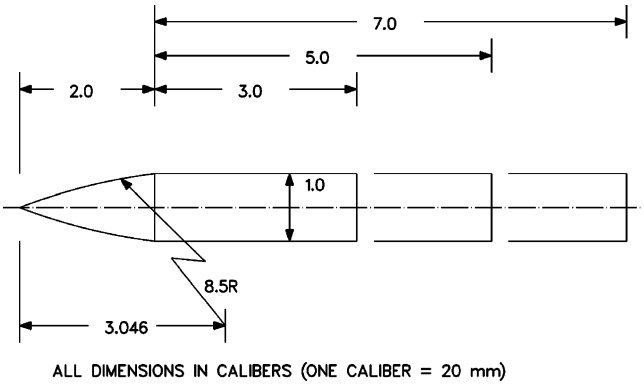

Fig. 4 Schematic of Army–Navy Spinner Rocket configuration.

Ogive-Cylinder Results

The computational approach was applied to a secant-ogive cylinder body [designated as the Army–Navy Spinner Rocket (ANSR)] shown in Fig. 4. Sample results for Mach 2.5, sea-level atmospheric conditions ($Re_D = 1.1 \times 10^6$) are shown as an example, although other supersonic velocities, Reynolds numbers, and geometries were considered during the course of the study. The results presented here are representative of the other flight conditions examined.

For the force coefficients, the deviation or error in the application of Sacks's relations is defined in Eq. (19). The deviation Δ_1 represents the difference between the right-hand and left-hand sides of Eq. (4):

$$\Delta = C_{N_{\dot\alpha}} - C_{m_\alpha} - C_{N_q} \equiv \Delta_1 \tag{19}$$

Note that by simple algebraic manipulations, the following relations that are algebraically equivalent to Eq. (19) are found:

$$\Delta = \left[C_{N_q} + C_{N_{\dot\alpha}}\right] - C_{m_\alpha} - 2C_{N_q} \equiv \Delta_2 \tag{20}$$

$$\Delta = 2C_{N_{\dot\alpha}} - C_{m_\alpha} - \left[C_{N_q} + C_{N_{\dot\alpha}}\right] \equiv \Delta_3 \tag{21}$$

Essentially, these deviations are a measure of the accuracy of the Sacks's relations shown in Eqs. (4), (6), and (8). It could be argued that the differences Δ_1, Δ_2, and Δ_3 are numerical errors that are not representative of physical phenomena. However, the deviation Δ can be computed independently in three different ways. The deviation Δ_1 is computed using the individual damping coefficients C_{N_q} and $C_{N_{\dot\alpha}}$ obtained independently from two different types of helical motion, while Δ_2 and Δ_3 are computed from the pitch-damping coefficient sum $C_{N_q} + C_{N_{\dot\alpha}}$ and one of the two individual damping coefficients C_{N_q} and $C_{N_{\dot\alpha}}$, respectively. The importance of having three independent methods of determining Δ is to demonstrate that the deviation is not due to an error in the prediction of any one of the three damping coefficients.

Similar expressions for the deviation of the moment coefficients $\bar{\Delta}$ can also be obtained and are shown in Eqs. (22–24):

$$\bar{\Delta} = C_{m_{\dot\alpha}} - C_{2m_\alpha} - C_{m_q} \equiv \bar{\Delta}_1 \tag{22}$$

$$\bar{\Delta} = \left[C_{m_q} + C_{m_{\dot\alpha}}\right] - C_{2m_\alpha} - 2C_{m_q} \equiv \bar{\Delta}_2 \tag{23}$$

$$\bar{\Delta} = 2C_{m_{\dot\alpha}} - C_{2m_\alpha} - \left[C_{m_q} + C_{m_{\dot\alpha}}\right] \equiv \bar{\Delta}_3 \tag{24}$$

Figure 5 shows the computed deviation for the force coefficient obtained from Eqs. (19–21) as a function of longitudinal distance from the nose. Here, the body has been lengthened to 20 calibers to more clearly illustrate the variation of the deviation along the body length. Results are obtained from a single computation of a 20-caliber-long body. Values of the force coefficients at intermediate body axial locations are obtained by integrating the force distribution

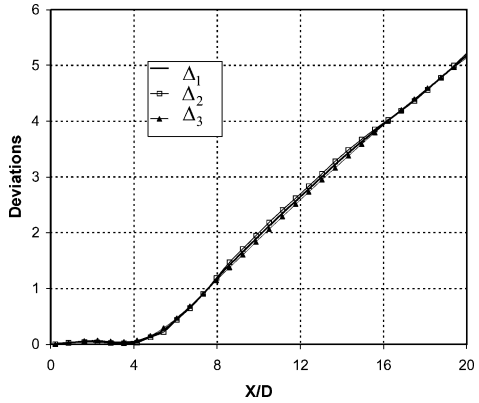

Fig. 5 Comparison of the three computed deviations Δ_1, Δ_2, and Δ_3 as a function of longitudinal distance from the nose.

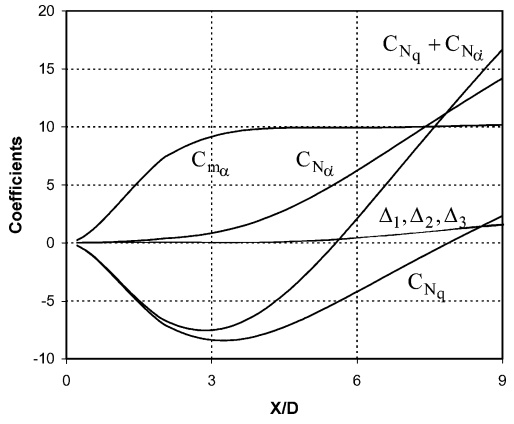

Fig. 6 Comparison of the longitudinal distribution of the three computed deviations Δ_1, Δ_2, and Δ_3 relative to the damping-force coefficients; $x_{cg}/L = 0.5598$, $L/D = 9$.

from the nose to the corresponding axial location. The results shown in Fig. 5 can be interpreted either as the distribution of the force deviation as a function of axial position for a fixed length body or as the force deviation as a function of body length. Both interpretations are equivalent under the assumptions associated with the space-marching approach used here.

There is very good correlation between the three different methods of computing Δ, suggesting that the deviation is representative of a physical effect rather than simply numerical error. The deviation is very small over the nose and begins to grow in a linear fashion a couple of body diameters aft of the nose. The deviation (for the force) can be shown to be independent of c.g. position using the c.g. translation relations for the individual force coefficients. This was also confirmed by varying the c.g. position in the computations as well. The computed deviation was also found to be somewhat dependent on nose length and Mach number, although the results shown are representative of the trends observed for the other flight conditions.

Figure 6 shows the distribution of the computed deviations for the force Δ_1, Δ_2, and Δ_3 compared with the distribution of the individual pitch-damping coefficients and the pitch-damping sum along the length of the body. Relative to $C_{N_{\dot\alpha}}$ and the pitch-damping force sum, the deviation is quite small. The distribution of the deviation is also small compared with the pitch-damping force coefficient C_{N_q} except near the end of the body where C_{N_q} itself is nearly zero. Equation (4) shows that, according to Sacks's relation, the difference between $C_{N_{\dot\alpha}}$ and C_{N_q} is the pitching-moment coefficient C_{m_α}. This is also graphically shown in Fig. 6. Near the nose of the body, the difference between the two damping coefficients $C_{N_{\dot\alpha}}$ and C_{N_q} increases at nearly the same rate as the pitching moment coefficient. On the aft portion of the body, the pitching-moment coefficient is nearly constant, and the difference between $C_{N_{\dot\alpha}}$ and C_{N_q} becomes relatively constant.

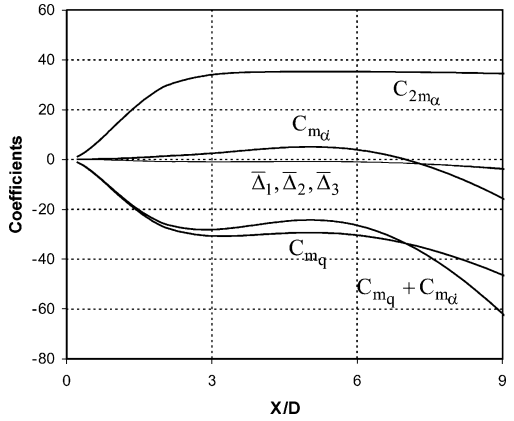

Fig. 7 Comparison of the longitudinal distribution of the three computed deviations $\bar{\Delta}_1$, $\bar{\Delta}_2$, and $\bar{\Delta}_3$ relative to the damping-moment coefficients; $x_{cg}/L = 0.5598$, $L/D = 9$.

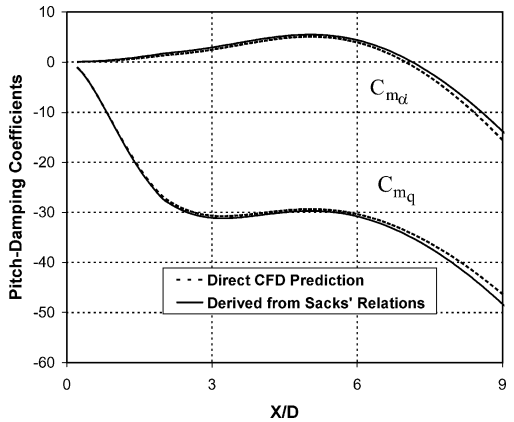

Fig. 8 Comparison of the damping-moment coefficients distributions predicted from Sacks's relations with CFD predictions; $x_{cg}/L = 0.5598$, $L/D = 9$.

Figure 7 shows the distribution of the computed deviation for the moment relative to the three damping-moment coefficients and the pitching second-moment coefficient along the length of the body. Again, there is very good correlation between the three methods for computing the deviation. The computed deviation is small compared to individual damping-moment coefficients and to the pitch-damping moment sum. Sacks's relation for the moment [Eq. (5)] shows that the difference between $C_{m_{\dot\alpha}}$ and C_{m_q} is the pitching second-moment coefficient C_{2m_α}. This also can be seen in Fig. 7. In a sense, Figs. 6 and 7 provide some measure of the expected error in applying Sacks's relations to obtain the various damping-moment coefficients given that normal-force distribution (or C_{m_α} and C_{2m_α}) and one of the pitch-damping coefficients is known.

The most likely application of Sacks's relations in practical situations is to compute the individual damping coefficients from the pitch-damping coefficient sum because the pitch-damping moment sum is much easier to measure. Through simple algebraic manipulations of Eqs. (7) and (9), the following form of the Sacks relations can be obtained:

$$C_{m_{\dot\alpha}} = \left(\left[C_{m_q} + C_{m_{\dot\alpha}}\right] + C_{2m_\alpha}\right)/2 \tag{25}$$

$$C_{m_q} = \left(\left[C_{m_q} + C_{m_{\dot\alpha}}\right] - C_{2m_\alpha}\right)/2 \tag{26}$$

Figure 8 shows the longitudinal distribution of the pitch-damping-moment coefficients C_{m_q} and $C_{m_{\dot\alpha}}$ obtained by applying Sacks's relationships using the pitch-damping-moment coefficient sum $[C_{m_q} + C_{m_{\dot\alpha}}]$ and the second-moment coefficient of the normal force C_{2m_α}. Here, CFD has been used to compute both $[C_{m_q} + C_{m_{\dot\alpha}}]$ and C_{2m_α}. The results from the application of these relations are compared with the CFD predictions of the individual damping coefficients. The coefficients C_{m_q} and $C_{m_{\dot\alpha}}$ are overpredicted and

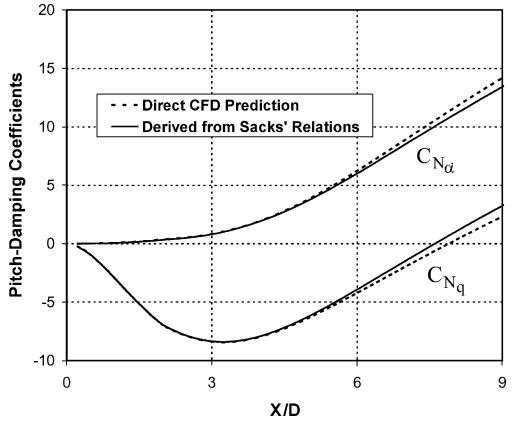

Fig. 9 Comparison of the damping-force coefficient distributions predicted from Sacks's relations with CFD predictions; $x_{cg}/L = 0.5598$, $L/D = 9$.

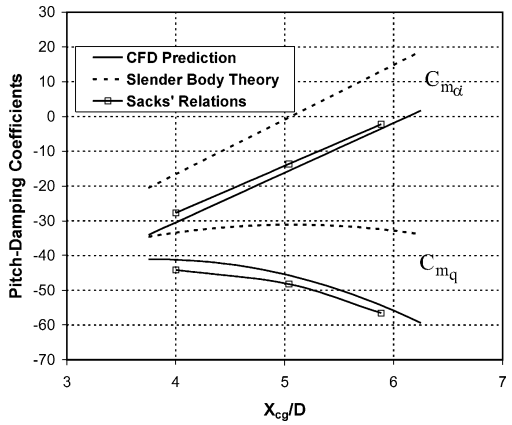

Fig. 10 Comparison of the predicted damping-moment coefficients with CFD and slender-body theory results; $L/D = 9$.

underpredicted by about 5 and 12%, respectively, although the absolute error is similar for both coefficients. The distribution of the damping coefficients over the body is also very well predicted.

Similar analysis can be performed for the force coefficients. Figure 9 shows the comparison of the longitudinal distributions of the individual pitch-damping-moment coefficients C_{N_q} and $C_{N_\dot{\alpha}}$ predicted using the form of Sacks's relations in Eqs. (27) and (28) with direct CFD predictions. The distribution of the force coefficients along the body is very well predicted using Sacks's relations:

$$C_{N_\dot{\alpha}} = \left(\left[C_{N_q} + C_{N_\dot{\alpha}}\right] + C_{m_\alpha}\right)/2 \tag{27}$$

$$C_{N_q} = \left(\left[C_{N_q} + C_{N_\dot{\alpha}}\right] - C_{m_\alpha}\right)/2 \tag{28}$$

Figure 10 shows the results for the individual pitch-damping coefficients for various CG positions for the body with the length-to-diameter ratio (L/D) of 9 at Mach 2.5 obtained by applying Eqs. (25) and (26). The results are compared with CFD results and with direct slender-body theory results. There is very good correlation of the results obtained with Sacks's relations and the CFD results, and the results are a significant improvement over the slender-body theory.

For the results shown in Figs. 8 and 9, comparisons have been made between the force and moment distributions along the body. This was done because these distributions are easily extracted from the computational results, and they allow detailed examination of the performance of Sacks's relations. It must be emphasized that it is not necessary to obtain the pitch-damping force and moment distributions in order to apply Sacks's relations because they work for the global force and moment coefficients as well. This is particularly important to consider when the source of the pitch-damping-coefficient data is an experiment in which only global coefficients are typically

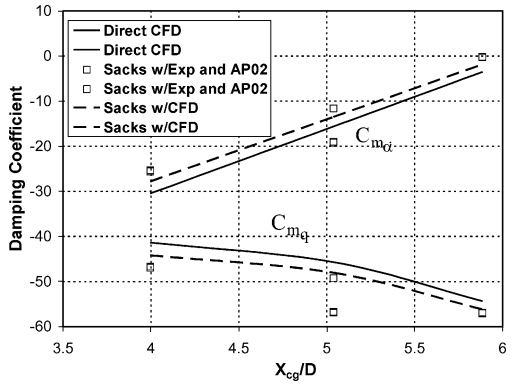

Fig. 11 Comparison of the damping-moment coefficients derived from experimental data or CFD using Sacks's relations with direct CFD prediction; $L/D = 9$.

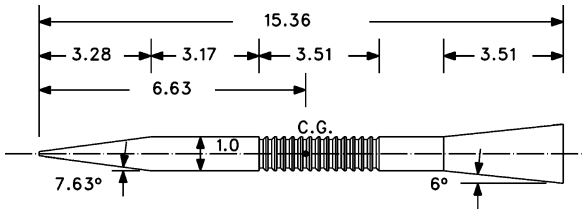

Fig. 12 Schematic of the flared projectile geometry; all dimensions in calibers (1 caliber = 8.28 mm).

available. However, Sacks's relations do require the normal-force distribution to determine C_{2m_α} because generally only the normal force and pitching moment are available as global coefficients from many sources. In lieu of more sophisticated computational methods for determining the normal-force distribution, fast-design aeroprediction codes[3] should provide acceptable accuracy for a variety of flight vehicle geometries.

To demonstrate the use of Sacks's relations when only global forces and moments are available, pitch-damping-moment coefficient sum data from range firings of the ANSR have been used to estimate the individual pitch-damping-moment coefficients using Sacks's relations. The normal-force distribution from the fast-design aeroprediction code AP02[3] has been used to predict C_{2m_α}. Figure 11 shows the individual pitch-damping coefficients predicted from Sacks's relations [Eqs. (25) and (26)] using experimental measurements of the pitch-damping-coefficient sum and C_{2m_α} obtained from AP02. The results are compared with direct CFD predictions of the individual damping coefficients as well as the results obtained from Sacks's relation using CFD predictions of the pitch-damping-coefficient sum and C_{2m_α} shown in Fig. 10. The experimentally derived values of the individual pitch-damping coefficients compare well with the predicted results. The results also indicate that the biggest source of error is produced by the uncertainty in the experimentally derived pitch-damping-moment coefficient rather than the error in Sacks's relations. (The pitch-damping data used here are from a highly regarded data set and are representative of the expected accuracy for the pitch-damping coefficient sum from range firings.)

Flared Projectile Results

The performance of Sacks's relations was also examined for a flared projectile geometry shown in Fig. 12. Direct CFD predictions of the pitch-damping-coefficient sum have been validated previously for this configuration using the same method described previously.[15] For the current paper, additional CFD predictions of the individual pitch-damping coefficients were also performed for flight velocities between Mach 2 and Mach 5 for sea-level atmospheric conditions ($Re_D = 4.5 \times 10^5$ and 1.125×10^6, respectively).

Figure 13 shows the longitudinal distribution of the computed deviations of the moment determined from Eqs. (22–24) compared

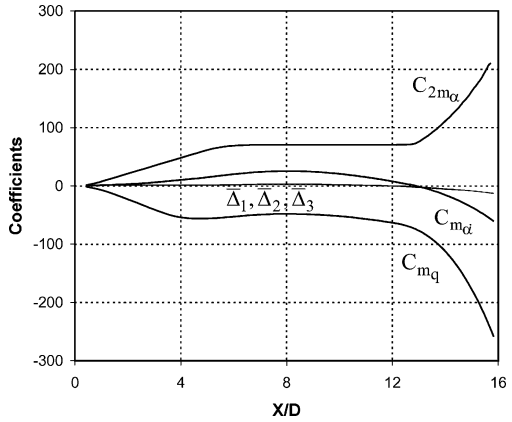

Fig. 13 Comparison of the longitudinal distribution of the three computed deviations $\bar{\Delta}_1$, $\bar{\Delta}_2$, and $\bar{\Delta}_3$ relative to the damping-moment coefficients, flared projectile, Mach 2.

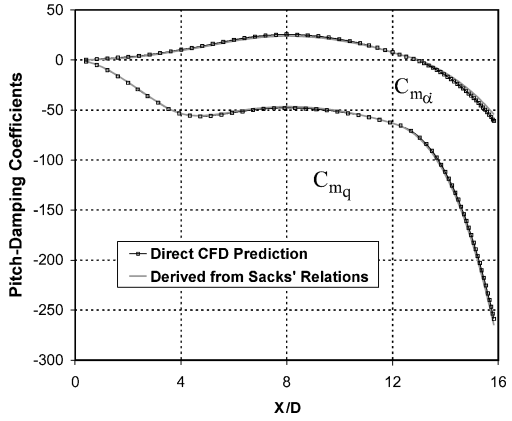

Fig. 14 Comparison of the damping-moment-coefficient distribution predicted from Sacks's relations with CFD predictions, flared projectile, Mach 2.

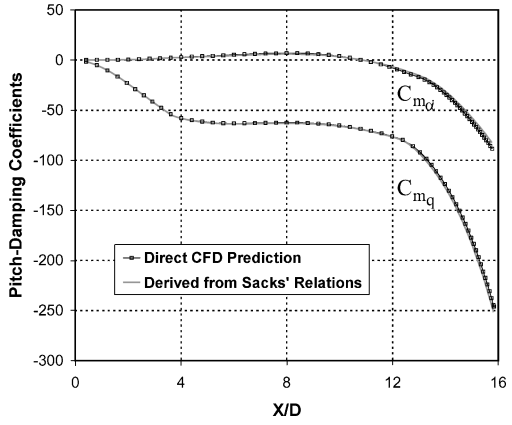

Fig. 15 Comparison of the damping-moment-coefficient distribution predicted from Sacks's relations with CFD predictions, flared projectile, Mach 5.

with longitudinal distribution of the individual pitch-damping coefficients predicted using CFD at Mach 2. Again, the deviation over the body is small compared to the pitch-damping coefficients, even on the afterbody where both the geometry and moment coefficients are changing significantly. Similar results were found at the other flight velocities.

Similar to the results for the secant ogive/cylinder configuration, the form of Sacks's relations embodied in Eqs. (25) and (26) was applied to determine the individual pitch-damping coefficients from the pitch-damping-moment-coefficient sum and the pitching-

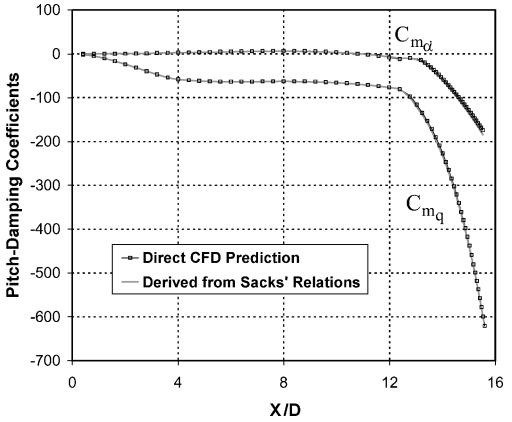

Fig. 16 Comparison of the damping-moment-coefficient distribution predicted from Sacks's relations with CFD predictions, 15-deg flared projectile, Mach 5.

second-moment coefficient for the flared projectile geometry. Comparisons were made with direct CFD predictions. Figures 14 and 15 show comparisons of the longitudinal distribution of the individual pitch-damping-moment coefficients at Mach 2 and 5, respectively, for the flared projectile geometry. Very good agreement between the results obtained by applying Sacks's relations and direct CFD predictions is found. Additional results for the same flared projectile with the 6-deg flare replaced by a 15-deg flare were also obtained and are shown in Fig. 16. Despite a nearly doubling of the pitch-damping coefficient due to the larger flare, the Sacks's relations results are in very good agreement with the direct CFD predictions.

Conclusions

In conclusion, the results presented here indicate that Sacks's pitch-damping relations are only strictly valid under the context of the theory from which they were originally developed. They do, however, provide a reasonably good means of estimating the pitch-damping coefficients when one of the three pitch-damping coefficients can be determined. The most likely practical use of these relations might be to provide estimates of the individual pitch-damping coefficients using values of the pitch-damping-coefficient sum determined from some other source, such as experimental data and engineering estimation approaches or when the additional expense of the separate computational fluid dynamics computations of the individual pitch-damping coefficients is not justified. In some cases, it appears that the error in applying these relationships is smaller than the error associated with generating the initial pitch-damping coefficient (such as with engineering estimation approaches) from which the other two damping coefficients are derived using Sacks's relations.

Applying Sacks's relations to determine the individual pitch-damping coefficients from the pitch-damping sum represents only one possible application of Sacks's relations. These relations could also benefit theoretical developments because theories for predicting the pitch-damping coefficients need only focus on a single damping coefficient. The other damping coefficients could then be obtained from Sacks's relations. Such an approach has been already used as an estimation procedure for the damping coefficients.[6] In this work, the distribution of $C_{N_{\dot{\alpha}}}$ along the body is predicted using slender-body theory with empirically based corrections. The damping coefficient C_{N_q} can then be obtained from Sacks's relations. Once the damping force distributions are known, the damping moments can be easily obtained by integration of the force loadings. Improvements in the estimates of C_{N_q} from Sacks's relations can also be obtained by correlating the error Δ as well, an approach used in Ref. 6 to further improve the estimates of C_{N_q}.

Finally, in the current paper only axisymmetric configurations in supersonic flight have been considered. The theory from which Sacks derived the relations considered here is applicable to both wingless and winged vehicles. Further research is still required to

assess the performance of Sacks's relations for winged vehicles and for other flight velocity regimes.

References

[1]Sacks, A. H., "Aerodynamic Forces, Moments, and Stability Derivatives for Slender Bodies of General Cross Section," NACA TN 3283, Nov. 1954, p. 27.

[2]Bryson, A. E., Jr., "Stability Derivatives for a Slender Missile with Application to a Wing-Body-Vertical-Tail Configuration," *Journal of the Aeronautical Sciences*, Vol. 20, No. 5, 1953, pp. 297–308.

[3]Moore, F. G., and Hymer, T. C., "The 2002 Version of the Aeroprediction Code: Part I—Summary of New Theoretical Methodology," U.S. Naval Surface Warfare Center, Rept. NSWCDD/TR-01/108, Dahlgren, VA, March 2002.

[4]Vukelich, S. R., and Jenkins, J. E., "Missile DATCOM: Aerodynamic Prediction on Conventional Missiles Using Component Build-up Techniques," AIAA Paper 84-0388, Jan. 1984.

[5]Whyte, R. E., "Spinner—A Computer Program for Predicting the Aerodynamic Coefficients of Spin Stabilized Projectiles," General Electric Co., Class 2 Rept. 69APB3, Burlington, VA, Aug. 1969.

[6]Danberg, J. E., and Weinacht, P., "Approximate Computation of Pitch-Damping Coefficients," AIAA Paper 2002-5048, Aug. 2002.

[7]Sigal, A., "Correlation of the Damping in Pitch Stability Derivatives for Body-Tail Configurations," AIAA Paper 94-3482, Aug. 1994.

[8]Weinacht, P., Sturek, W. B., and Schiff, L. B., "Navier–Stokes Predictions of Pitch-Damping for Axisymmetric Projectiles," *Journal of Spacecraft and Rockets*, Vol. 34, No. 6, 1997, pp. 753–761.

[9]Weinacht, P., "Navier–Stokes Predictions of the Individual Components of the Pitch-Damping Sum," *Journal of Spacecraft and Rockets*, Vol. 35, No. 5, 1998, pp. 598–605.

[10]Park, S. H., Kim, Y., and Kwon, J. H., "Prediction of Damping Coefficients Using the Unsteady Euler Equations," *Journal of Spacecraft and Rockets*, Vol. 40, No. 3, 2003, pp. 356–362.

[11]Schiff, L. B., and Steger, J. L., "Numerical Simulation of Steady Supersonic Viscous Flow," *AIAA Journal*, Vol. 18, No. 12, 1980, pp. 1421–1430.

[12]Weinacht, P., and Sturek, W. B., "Computation of the Roll Characteristics of a Finned Projectile," *Journal of Spacecraft and Rockets*, Vol. 33, No. 6, 1996, pp. 769–775.

[13]Baldwin, B. S., and Lomax, H., "Thin Layer Approximation and Algebraic Model for Separated Turbulent Flows," AIAA Paper 78-257, Jan. 1978.

[14]Beam, R., and Warming, R. F., "An Implicit Factored Scheme for the Compressible Navier–Stokes Equations," *AIAA Journal*, Vol. 16, No. 4, 1978, pp. 85–129.

[15]Weinacht, P., "Navier–Stokes Predictions of Pitch-Damping for a Family of Flared Projectiles," AIAA Paper 91-3339, Sept. 1991.

R. Cummings
Associate Editor